JOURNAL OF PROPULSION AND POWER
Vol. 11, No. 4, July–August 1995

Vortex-Shedding Phenomena in Solid Rocket Motors

François Vuillot*
ONERA, 92322 Chatillon, France

In the past 20 years, periodic vortex shedding as a source of acoustic energy inside solid propellant rocket motors has been continuously studied, in connection with several motors that exhibited oscillatory behaviors although they were predicted stable by means of conventional linear stability methods. On that subject, correlations through Strouhal numbers are commonly used. In this article, the meanings of various Strouhal number definitions are discussed. The basic mechanisms for sound production in ducts or chambers are then discussed through simple tools, such as the linear hydrodynamic stability analysis, Flandro's method and the acoustic balance technique, which provide good insights into the physics of the phenomenon. Necessary conditions for vortex-shedding-driven motors are then arrived at and illustrated by actual firing results. Finally, the full numerical approaches are shown to provide unprecedented insight into the mechanisms behind the vortex-shedding phenomenon and are believed to open the way to quantitative predictions of frequencies and oscillatory levels.

Nomenclature

a = dimensionless wave number $\alpha\delta$, speed of sound
B = integration constant in the hydrodynamic stability analysis
c = dimensionless angular frequency, $2\pi f\delta/\Delta U_e$
D = internal diameter
d = diameter, deflection of inhibitor ring, Fig. 11
E_N^2 = $\int_V \bar{p}_N^2 \, dv$
f = frequency
i = $\sqrt{-1}$
$\boldsymbol{i}, \boldsymbol{j}, \boldsymbol{k}$ = unit normal vectors
K_D, K_U, K_V = proportionality constants, Sec. VI
k = acoustic wave number
L = length
ℓ = standoff distance
M = Mach number
p = pressure
Re = Reynolds number
S = surface, surface area
St = Strouhal number
t = time
U_v = vortex displacement velocity, $U_v/\Delta U_e = c^r/a^r$
u, U = velocity, axial velocity
v, V = transverse velocity, volume
x, y = axial, transverse coordinates
α = spatial wave number, Sec. III, linear growth rate
ΔU_e = shear layer velocity difference
δ = boundary-layer thickness
ζ = nondimensional hydrodynamic vorticity
λ = wavelength, $\lambda_v = 2\pi\delta/a^r$: vortical wavelength
ν = kinematic viscosity
ξ = spatial variation of nondimensional hydrodynamic vorticity
ρ = density
Φ = phase
Ω = steady-state vorticity
ω = angular frequency

Subscripts
cr = critical value
e = external value
i = value at impact
m/a = maximum amplification
N = reference acoustic mode
v = vortex characteristic
0 = reference state

Superscripts
r, i = real, imaginary parts of a complex number
$'$ = unsteady component
$''$ = acoustic component, Sec. IV
$-$ = mean value
$\sim$ = spatial variation of an unsteady component

Received Aug. 25, 1994; revision received Feb. 8, 1995; accepted for publication Feb. 16, 1995.
*Project Manager, Energetics Department. Member AIAA.

I. Introduction

IN the past 20 years, periodic vortex shedding as a source of acoustic energy inside solid propellant rocket motors has been continuously studied, in connection with oscillatory behaviors of several motors that were predicted stable by means of conventional linear stability methods, such as the acoustic balance.

The mechanisms for sound production from flows in ducts or chambers have been known for many years and are commonly used in musical instruments. The first suggestion of acoustic mode excitation by vortex shedding in solid rocket motors was made by Flandro and Jacobs[1] who emphasized the motor instability risk linked to the hydrodynamic instability of the mean flow sheared regions. It seems that the first evidence of vortex-shedding-driven oscillations were encountered in motors with complex grain geometry, used for ballistic missiles upper stages,[2–4] as unanticipated and unexplained oscillatory behavior. The most noticed characteristic was decreasing frequencies, as the grain burned back, which departed from computed acoustic frequencies. This was later interpreted as an indication of the dependence of the frequency upon the gas flow velocity, which is now a widely accepted signature of vortex-shedding-driven oscillations. Reference 4 contains a detailed summary of that problem.

Most of the recent research efforts to understand the mechanisms for vortex-shedding-driven oscillations were conducted in connection with the developments of large segmented solid-propellant boosters for space applications, such

as the U.S. Space Shuttle and Titan boosters, and more recently, the European Ariane 5 booster. All of these motors developed, at distinctive times into the firing, low-level but sustained pressure and thrust oscillations on their first longitudinal modes, although they were predicted stable by classical stability prediction codes. Zero-peak relative amplitudes were typically less than 0.5% for pressure oscillations and less than 5% for thrust oscillations. Although such levels did not seem to jeopardize motor operation, the low frequencies (associated with the large dimensions of these motors) of the potentially unstable modes, made the possible coupling with the launcher structural modes a serious point of concern. The possible scatter from motors-to-motors was also a matter of concern. This situation motivated numerous research works in the U.S., starting in the late 1970s and early 1980s.[5–10] The occurrence of vortex shedding in such geometries, as well as the predominant role of inhibitor rings protruding into the chamber, was clearly identified by the works at the Chemical System Division of United Technology Corp., through cold-flow simulation of a scaled-down Titan booster.[8] This work was essential in several aspects: first, it actually measured vortices by means of hot wire anemometry and identified the "active pair" among the several Titan segment inhibitor rings; second, it clearly measured the frequency shifts associated with variations of the mean flow velocity (obtained through variations of the choked nozzle throat area), establishing that the ratio f/U remained constant; third, it demonstrated the reality of the acoustic coupling phenomenon, since head-end pressure oscillations were found to be correlated to velocity oscillations downstream of the first active inhibitor ring. However, the importance of the vortex impingement in the overall coupling seemed to have been overlooked and correlations were proposed through a Strouhal number defined as

$$St_1 = fD/U \tag{1}$$

with D being the inhibitor ring i.d. and U the gas flow velocity. A value of St_1 of the order of or less than unity was considered as critical for the appearance of instabilities.[8] Finally, it became clear that the segmented nature (that produces regions of highly sheared flow, due to port area discontinuities and protrusion of inhibitor rings), as well as the large length-to-diameter ratio of these motors made them prone to vortex-shedding-driven oscillations at frequencies close to the first longitudinal mode frequencies.

The role of inhibitor rings (acting as diaphragms) was further documented through cold-flow studies.[7,11–16] These studies demonstrated the reality of sound generation through vortex shedding, in motor-like configurations, and led to interesting discussions on the role of acoustic coupling. Going through that particular matter requires some background, which will be given in Sec. II.

Flandro,[17] extending the work of Ref. 1, proposed a linearized approach, based on the hydrodynamic stability analysis, to evaluate the vortex-shedding risk in solid propellant rocket motors and to incorporate a corresponding driving term in linear acoustic balance codes. To date, this method appears to be the only one to attempt to correct available linear stability prediction codes for the effects of vortex shedding. This method will be presented in Sec. IV.

More recently, in Europe, the development of the Ariane 5 large segmented booster MPS P230 (comprising three seg-

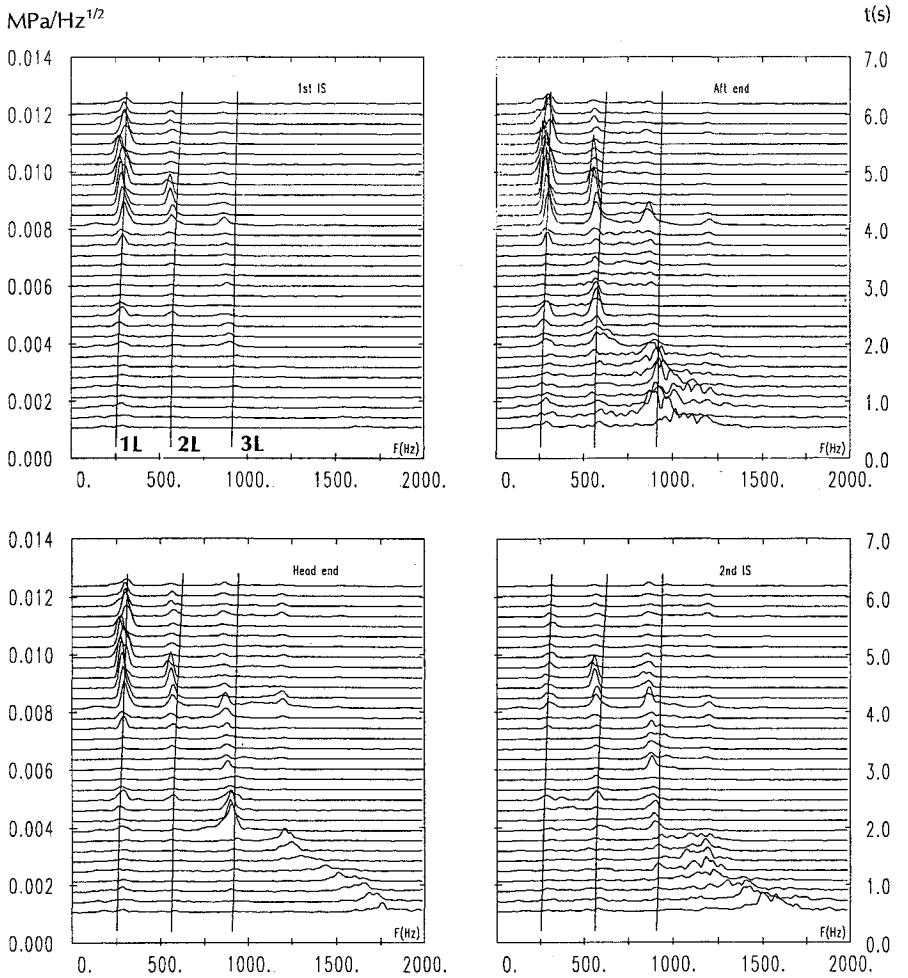

Fig. 1 Illustration of the vortex-shedding signature, from psd of pressure measurements from a 1/15-scale parametric motor.

ments), spurred a multiteam research work on the particular subject of vortex-shedding-driven oscillations, prior to the first full-scale firing. This research effort included both experiments on parametric subscale (1/15) segmented motors and theoretical developments.[18–21] The parametric experimental program test-fired several intersegment arrangements.[20] Figure 1 displays a waterfall plot of power spectral density (psd) of unsteady pressure measurements. These were recorded during the experimental campaign, at four locations inside the motor (head-end, first intersegment, second intersegment, and aft-end). On that figure, the vortex-shedding signature is clearly visible. On the theoretical part, application of Flandro's linearized model to the Ariane 5 MPS P230 motor was carried out[20] and concluded of a possible vortex-shedding driving, from the second inhibitor ring. This prediction later proved to be qualitatively correct and to this author's knowledge is the only attempt to apply Flandro's method to actual motors. It must be noted that the simplified methods provide the necessary understanding of the physical mechanisms responsible for the vortex-shedding phenomenon in solid rocket motors and can be used to derive qualitative assessments of potentially unstable motor configurations (see Sec. VI). However, the limitations of the simplified approaches are clearly apparent (see Sec. IV), without mentioning the evident complexity of the phenomenon itself, and motivated the consideration of full numerical simulation of vortex shedding, as was already done in similar fields.[22]

First, the feasibility of the full numerical approach was established at ONERA, on a simple geometry motor (see Ref. 18 and Sec. VII), and first validations against experiments are discussed in Refs. 20 and 21. Application to actual motors became then possible, and provided unprecedented insight into the phenomena behind vortex-shedding-driven oscillations.[18–21] In a particular case, corresponding to one 1/15-scale segmented motor, vortex pairing was computationally observed, and could explain the different frequencies recorded at the head-end and aft-end of the motor.[20] This was an important step, since the fact that different frequencies could be observed at the two ends of a motor violated the acoustic mode concept that is at the basis of all stability prediction codes. At the same time, limited work was carried out in the U.S.[23,24] that emphasized the promises of the full numerical approach. Finally, the potential of the numerical approach, in terms of predictions of oscillatory frequencies as well as pressure and thrust oscillatory levels, up to the full scale, will be discussed in Sec. VII.

II. Acoustic Coupling and Strouhal Numbers

The term acoustic coupling implies that the shedding of the vortices can be influenced by the chamber acoustics. Although this seems natural, early experiments[11,12] seemed to demonstrate that this was not the case. To discuss that matter, it is useful to recall that vortex shedding by a wire in uniform relative motion in an open medium was clearly identified, since the early work of V. C. Strouhal (see Ref. 25) that introduced the so-called Strouhal number:

$$St_2 = fd/U \tag{2}$$

where f is the shedding frequency, d is the wire diameter, and U is the relative velocity of the gas to the wire. The Strouhal number was found to be a function of the Reynolds number, $Re = Ud/\nu$, and of wire properties.

The physical mechanism behind vortex shedding is the instability of shear layers in the gas flow. The hydrodynamic stability analysis will be detailed in Sec. III. For the present discussion it suffices to say that this analysis introduces a Strouhal number based on shear layer characteristics, such as its thickness δ, and the velocity difference across it ΔU_e:

$$St_3 = f\delta/\Delta U_e \tag{3}$$

The inflectional shear layer is found to be unstable, for all Reynolds numbers, for a large frequency range ($[0 - f_{cr}[) \cdot f_{cr}$ corresponds to a critical Strouhal number, for a given velocity profile and for a given Reynolds number, above which no instability (in the linear sense) can develop.

In a closed cavity, such as a solid propellant motor chamber, several other length scales must be taken into account and somewhat complicate the matter. First, there are the cavity dimensions, such as L and D, which govern the chamber acoustic mode frequencies and the mean flow velocity. Second, in closed cavities it is common to encounter a new length-scale ℓ characteristic of a standoff distance, in the direction of the mean flow of velocity U, which is used to define a new Strouhal number as

$$St_4 = f\ell/U \tag{4}$$

The distance ℓ separates the point of emission of the vortices from an impingement point, located downstream. This latter point can be the second diaphragm of a diaphragm pair or the nozzle wall. This introduces a possible coupling between the vortex shedding and the acoustics of the chamber, through a phase relationship between the impinging vortex and the acoustic field. Figure 2 illustrates such a situation: vortex impingement creates a pressure wave; if this pressure wave has the proper frequency and phase it can drive one of the chamber acoustic modes, which, in turn, will organize and modulate the shedding. Nomoto and Culick,[12] on the grounds of their experiment, argued that acoustic coupling or acoustic feedback should not be the important phenomenon in vortex shedding.

However, the reality of acoustic coupling was demonstrated by Blevins,[26] in the case of transverse modes, through acoustic forcing. Hourigan et al.[14] also observed acoustic coupling in the case of a diaphragm pair placed in a duct and of longitudinal modes. The setup of Ref. 14 was quite similar in principles to the one of Ref. 12, and the different conclusions by their authors could have an explanation in operating conditions. Reference 14 presents results for Strouhal numbers in the range 4–12, when based on Eq. (1) and the axial velocity upstream of the first diaphragm. These values correspond to the range 1–3, when converted in terms of axial velocity just above the first diaphragm (a contraction ratio of 4 is used), indicating that at least one vortex has time to travel from one diaphragm to the other during an acoustic cycle. Reference 12, which uses almost the same contraction ratio (3.92), presents results for lower Strouhal numbers, that is to say that the diaphragms may be too close to each other to permit the coupling mechanism to appear. In practical situations, the standoff distance is often sufficient for one or more vortices to take place between emission and impingement points. This makes possible acoustic feedback and acoustic coupling. In such conditions, it is possible to couple the shear layer instability to the acoustic frequency, provided it lies inside the instability range of the shear layer. This coupling, as illustrated by Fig. 2, is now believed to be essential in the

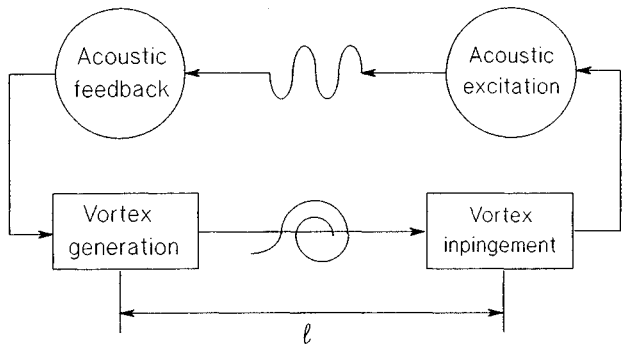

Fig. 2 Illustration of the acoustic coupling phenomenon.

so-called vortex-shedding instability in solid propellant motors. In the remainder of this article the term vortex-shedding-driven oscillations will thus refer to such acoustically coupled vortex-shedding-driven oscillations.

This coupling can establish itself through a variety of paths, corresponding to a different number of vortices. Unstable Strouhal numbers (i.e., leading to instabilities) actually express a phase relationship between vortices and the acoustic field at the impingement point. In that sense, discontinuous behavior can be anticipated and explained, as the phenomenon shifts from one path to another. References 15 and 16 provide a good illustration of this phenomenon and of the importance of the standoff distances. At this point, it is interesting to note that an efficient mean to suppress vortex-shedding-driven oscillations is to have the shear layer critical frequency smaller than the first acoustic mode frequency of the chamber. Such behaviors as frequency shifts and stabilization, were indeed computationally reproduced in Ref. 27.

To summarize, it can be said that several definitions for the Strouhal number exist: 1) $St = fD/U$, 2) $St = fd/U$, 3) $St = f\delta/\Delta U$, 4) $St = f\ell/U$, and may seem confusing. However, they correspond to different physical mechanisms, and thus bear different meanings: 2 and 3 are related to shear layer instability, as well as 1 in the case of solid rocket motor, whereas 4 is related to the acoustic coupling mechanism.

In a one-length-scale problem, such as the open medium case, definition 2 suffices to correlate the observed results, for a given class of flowfield. Definition 3 could also be used, with more generality, but it is less directly measurable, so that 2 is often preferred.

In several length-scale problems, such as closed cavity or solid rocket motors, definition 1 is the counterpart of definition 2: it is readily available to correlate the results, but it lacks generality in failing to take into account the proper relationship between D and δ (which may now vary during the firing), and the other length scales, such as ℓ, which characterizes the acoustic coupling mechanism. An alternative would be to correlate with definition 4, but this time the lack of generality would come from the failure to take into account the shear layer instability mechanism.

Vortex-shedding phenomenon in solid propellant rocket motors belongs to the multiple length-scale category of problems, and thus, none of the above Strouhal number definitions can be safely used alone to correlate the results. It must also be stressed that correlations through Strouhal numbers can have application limits, e.g., when the shear layer is not sufficiently isolated for the hydrodynamic stability analysis to be valid.

III. Hydrodynamic Stability

The hydrodynamic stability analysis relies on the linearization of the incompressible equations of motion, around a known mean flow [e.g., $u(t) = U + u'(t)$, with $|u'| << |U|$]. Further assumption of a parallel mean flow is usually made to ease the algebraic developments. This leads to the so-called Orr–Sommerfeld equation or the Rayleigh equation, if the viscosity is neglected. The interested reader is referred to Refs. 28 and 29 for a detailed description of the problem and solution methods. The validity of the parallel mean flow assumption can be questionned for applications close to the burning propellant surface where the strong gas injection renders the mean flow nonparallel. Reference 30 shows that the flow stability is greatly modified by the injection. However, for the applications presented hereafter, the velocity profiles that are considered are sufficiently away from the injecting surfaces for this assumption to be considered valid.

In the simplified case of one-dimensional propagation along the x axis, for a mean velocity profile given by $U(y)$, the small fluctuations are expressed as

$$u' = Bf(y)e^{i(\alpha x - \omega t)}$$

$$v' = B\varphi(y)e^{i(\alpha x - \omega t)}$$

$$p' = B\pi(y)e^{i(\alpha x - \omega t)}$$

B is an integration constant, $f(y)$, $\varphi(y)$, and $\pi(y)$ are the vortical fluctuation profiles across the shear layer. In general, α and ω are complex numbers. The temporal growth rate theory corresponds to α real and ω complex, while the spatial growth rate theory corresponds to α complex and ω real. The hyperbolic tangent profile has been studied theoretically by Michalke for an inviscid fluid,[31,32] for both the temporally and the spatially growing cases. The experiments by Freymuth,[33] on a laminar jet mixing layer, established good comparisons with the spatial stability theory. Reference 34 also studied the hyperbolic tangent profile and established a dependence of the spatial growth rate on the velocity ratio across the shear layer. For the spatial growth rate theory, for any given ω, the hydrodynamic stability computations yield: $\alpha = \alpha^r + i\alpha^i$ as the solution to an eigenvalue problem. From them, $f(y)$, $\varphi(y)$, and $\pi(y)$ can be obtained. These computations make use of nondimensional quantities defined as follows: $c^r = 2\pi f\delta/\Delta U_e$ and $a = \alpha\delta = a^r + ia^i$.

The hydrodynamic stability analysis will be illustrated on the simplified motor geometry of a computational test case used at ONERA to validate internal aerodynamic codes, which is fully described in Ref. 35. Figure 3 displays the geometry of this test case, and its 110 × 16 grid. The motor length is 270 mm, the chamber i.d. is 90 mm, and the overall grain length is 170 mm. This geometry naturally produces a sheared flow at the right-hand side (RHS) corner of the propellant grain ($I = 30$), due to the diverging injecting wall. It must be stressed that the shearing is the result of the injecting boundary (rather than of viscous boundary layers), which produces a rotational mean flow (e.g., $\partial U/\partial y \neq 0$), even for an inviscid description of the flow, since mass and momentum balances at the burning propellant surface force the flow to enter the chamber normally to the surface.[36] This is an important point to keep in mind, which has surprised many researchers from outside of the solid propellant community.

The hydrodynamic stability of this shear layer has been studied by means of a computer code from ONERA/CERT/DERAT,[37] that solves the incompressible Orr-Sommerfeld equation. Figure 4 displays the axial velocity profile (at station $I = 38$). Due to the limited number of grid points, the profile had to be smoothed. The smoothed profile was of the form: $u/\Delta U_e = A \tanh[a(y/\delta) + b] + c$, with: $A = 0.51735$, $a = 5.5302$, $b = -1.6876$, $c = 0.48312$, $\delta = 0.034$ m, $\Delta U_e = 265.1$ m/s.

The smoothed profile was then symmetrized in order to locate the inflection point at $y/\delta = 1/2$; this led to the following of new nondimensionalizing values: shear layer 99.9% thickness $\delta = 0.02024$ m, and velocity difference $\Delta U_e = 255.1$ m/

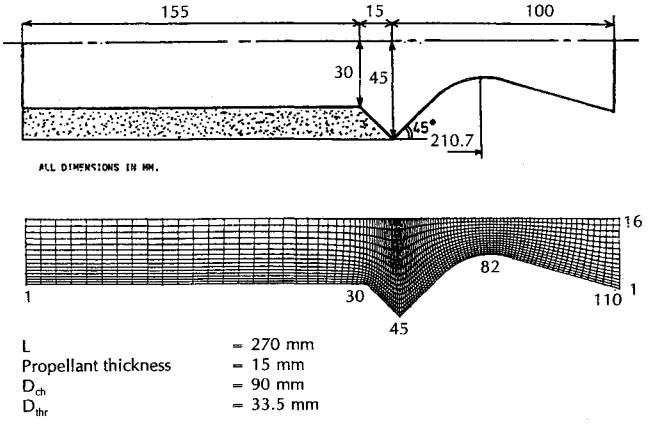

Fig. 3 Simplified test case.

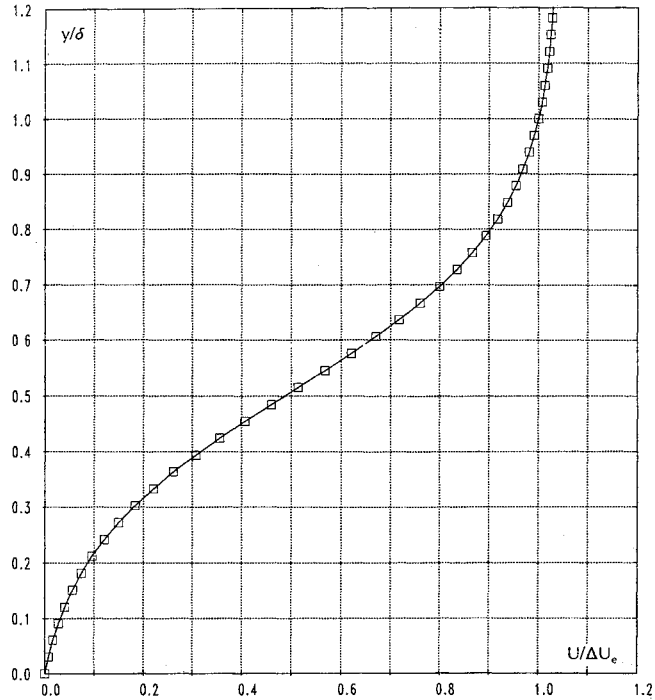

Fig. 4 Velocity profile of test case at station I = 38.

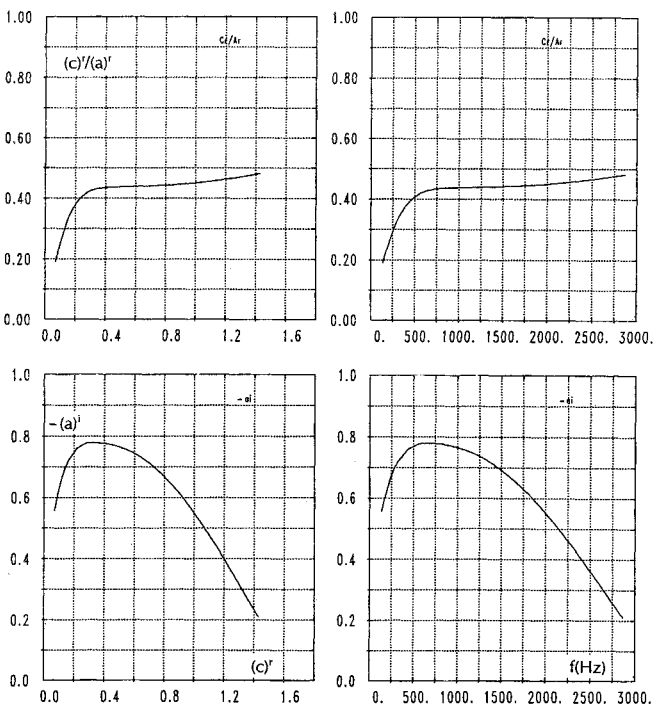

Fig. 5 Hydrodynamic stability analysis of the velocity profile of Fig. 4.

s. The corresponding Mach number difference is (for a typical speed of sound of 1075 m/s): $\Delta M_e = 0.24$, which stays in the incompressible range.

The resulting curves of a^r (or rather, c^r/a^r) and $-a^i$ as functions of frequency are given on Fig. 5. It appears that the unstable frequency range is roughly [0–3500 Hz[, with a frequency for maximum amplification close to $f_{m/a} = 750$ Hz. In dimensionless quantities the following values are obtained:

$$(c^r)_{m/a} = 0.30, \qquad (a^r)_{m/a} = 0.75$$

$$(a^i)_{m/a} = -0.78, \qquad (c^r)_{cr} \approx 1.60$$

From these curves, one can deduce the vortical wavelength: $\lambda_v = 2\pi\delta/(a^r)$, and the vortex velocity: $U_v/\Delta U_e = (c^r)/(a^r)$. The dimensionless critical frequency corresponds to a critical Strouhal number [Eq. (3)] of 0.26.

In the test case of Fig. 3, the vortices have no space to develop and the flowfield remains stable. This would not be the case if sufficient space were provided for the vortices to develop (see Sec. VI).

IV. Flandro's Method

Flandro's method[17] will be recalled here, because it is very useful to understand the mechanisms leading to vortex-shedding-driven oscillations. First, Flandro splits the flowfield in three parts: 1) the mean flowfield, 2) the acoustic motions (compressible and irrotational), and 3) the hydrodynamic motions (incompressible but rotational); each part has its own scaling. The method adds a body force in the momentum equation that is later used to introduce a localized vortex impingement effect (see step 4 discussed later in this article). When deriving the linearized equations, two distinct vortical flow effects are identified. The first one appears as a volume integral of the form

$$\int_V u' \cdot [u' \wedge (\nabla \wedge u)]\, dV$$

It is argued that this contribution is negligible.[17] The second effect comes from the body force, which yields a surface interaction, since it is concentrated at the location of vortex impact. It is argued[17] that this latter contribution, the so-called dipole effect, is the most significant. Although this approach is very physical, it must be stressed that it bears some arbitrariness in introducing a localized body force. This method can be summarized in four steps: 1) determination of the velocity profile of the shear layer supposed to be responsible for the hydrodynamic instability; 2) determination of the hydrodynamic stability of the velocity profile for the spatial growth rate theory; 3) for an acoustic mode of given frequency, coupling of the vortical flowfield with the acoustic field; and 4) choice of an impact surface where the pseudo-sound-field, associated with the vortical flow, will interact with the acoustic field. The first two steps are similar to the ones already described in Sec. III. The third step couples the hydrodynamic solution with the acoustic field (u'', p''), for a given mode frequency. The coupling procedure is based on the following first-order coupled equation for the nondimensional vorticity $\zeta = \xi e^{-i\omega t}$ (see Ref. 17):

$$\frac{\partial \zeta}{\partial t} = \frac{1}{M_e} \nabla \wedge (u'' \wedge \Omega) \tag{5}$$

where u'' is the acoustic velocity, nondimensionalized by the speed of sound, and Ω and M_e are the steady-state nondimensional vorticity and Mach number, respectively. For a pure cylindrical mode

$$u'' = i \frac{p_0''}{\rho_0 a_0^2} \sin\left[\frac{2\pi f}{a_0}\,\delta\left(x + \frac{X_0}{\delta}\right)\right] e^{-i\omega t} \boldsymbol{i} \tag{6}$$

here, the origin of the x axis (X/δ, in the hydrodynamic units) is located at the shear layer origin (X_0). The term $\nabla \wedge (u'' \wedge \Omega)$ becomes $(-\Omega \partial u''/\partial x)\boldsymbol{k}$, and a particular solution to (5) is simply

$$\xi_p = \frac{p_0''}{\rho_0 a_0^2}\,\Omega \cos\left[\frac{2\pi f}{a_0}\,\delta\left(x + \frac{X_0}{\delta}\right)\right]$$

Due to the linear nature of the problem, this solution is added to the hydrodynamic field ξ, which is known except for the integrating constant B: $\xi_{\text{total}} = \xi_p + B\xi$.

B can be found by imposing that ξ_{total} is zero at shear layer origin ($x = 0$, $y = \delta/2$):

$$B = -\frac{p_0''}{\rho_0 a_0^2}\frac{\Omega}{\xi_{(0,1/2)}}\cos\left(\frac{2\pi f X_0}{a_0}\right)$$

where $\xi_{(0,1/2)} = |\xi_0|e^{i\Phi(\xi_0)}$. The associated pressure field is $p'_v = B\pi(y)e^{i(\alpha x - \omega t)}$.

The fourth step permits the assessment of the vortex-shedding effect on the linear acoustic balance. For an impact surface at the distance ℓ from the shear layer origin, noting $\Delta\phi_i$ the hydrodynamic field phase difference between the origin and the impact surface ($\Delta\phi_i = \alpha^r\ell$), and taking $\pi(y) = 1$, which is a good approximation, from the hydrodynamic stability analysis, the pressure field p'_v is

$$\frac{p'_v}{\rho_0 U_c^2} = \frac{-p_0''}{\rho_0 a_0^2}\frac{\Omega}{|\xi_0|}e^{-\alpha^i\ell}\left(\cos\left(\frac{2\pi f X_0}{a_0}\right)\exp\{i[\Delta\Phi_i - \Phi(\xi_0)]\}\right) \tag{7}$$

The dipole effect, at the impact surface S_i, can be put in the form of a linear growth rate α_v that can be added to the linear growth rate computed by classical stability prediction programs (see Sec. V):

$$\alpha_v = \frac{\rho_0 a_0^2}{2E_N^2}\int_{S_i} p'_v \boldsymbol{u}''\cdot\boldsymbol{n}\,\mathrm{d}S, \quad \text{with} \quad E_N^2 = \int_V (p'')^2\,\mathrm{d}v$$

(in dimensional form, for an inward-pointing normal). A first estimation of the vortex-shedding effect can be obtained from the phase difference: $\Delta\phi_v = \phi(u'') - \phi(p'_v)$. From Eqs. (6) and (7), the phases of p'_v and u'' at the impact surface are

$$\phi(p'_v) = \phi(\cos[(2\pi f/a_0)X_0]\exp\{i[\Delta\Phi_i - \Phi(\xi_0) + \pi]\})$$

$$\phi(u'') = \phi\{\sin[(2\pi f/a_0)(X_0 + \ell)]\exp[i(\pi/2)]\}$$

Then $\Delta\phi_v = \phi(\xi_0) - \Delta\phi_i + (\varepsilon_2 - \varepsilon_1 - \frac{1}{2})\pi$, where ε_1 and ε_2 take values 0 or 1:

$$\varepsilon_1 = 1, \quad \text{if} \quad \cos[(2\pi f/a_0)X_0] < 0$$

$$\varepsilon_2 = 1, \quad \text{if} \quad \sin[(2\pi f/a_0)(X_0 + \ell)] < 0$$

Finally, the criterion for a destabilizing vortex-shedding effect is simply

$$90 < \Delta\phi_v < 270 \text{ deg}$$

meaning that p'_v and u'' have out-of-phase components. One can go one step further by actually computing α_v. Assuming that p'_v and u'' are constant on S_i, one can write

$$\alpha_v = -(\rho_0 a_0^2/2)[\mathrm{Re}(p'_v)]^2\,\mathrm{Re}(u''/p'_v)(S_i/E_N^2)$$

where Re( ) indicates the real part of a complex quantity. Then

$$\alpha_v = A|\cos[(2\pi f/a_0)X_0]||\sin[(2\pi f/a_0)(X_0 + \ell)]| \times \cos^2[\Delta\Phi_i - \phi(\xi_0)][-\cos(\Delta\phi_v)]$$

with

$$A = (a_0/2)p_0''^2\{M_c^2\Omega/|\xi_0|)(S_i/E_N^2)e^{-\alpha^i\ell}$$

It thus appears that α_v is the product of 1) a sign factor linked to $\Delta\Phi_v$, 2) a geometric factor that is a function of X_0, ℓ, the acoustic mode (represented by f and the X-axis origin at the head-end) and of the hydrodynamic field [represented by $\Delta\Phi_i$ and $\Phi(\xi_0)$], and 3) an amplitude factor A, which depends on $\alpha^i\ell$, M_c, Ω, . . .

It turns out that the coupling procedure is very sensitive to most of its input parameters. Indeed, the work done at ONERA has found that Flandro's method is extremely sensitive to most parameters (X_0, ℓ, f, . . .), raising the question of reliability and representativity.[18] In addition, the linear approach cannot give accurate frequency prediction, since the frequency is an input of the model. Lastly, it requires that the steady-state velocity profiles be known with a sufficient spatial resolution, to avoid uncertainties linked to the smoothing, needed for the hydrodynamic stability computations to converge to meaningful results. At this point, it must be stressed that the results of the hydrodynamic stability analysis are by themselves very valuable, in the sense that they provide the frequency above which the velocity profile is intrinsically stable (see Sec. III).

V. Remarks on the Acoustic Balance

The most classical approach used to assess the linear stability of solid propellant rocket motors is the acoustic balance method, first proposed by Hart and McClure,[38] and which was given its most practical form by Culick.[39–41] This method starts with an initial approximation of the acoustic modes of the cavity consisting of the burning surface, the propulsion system walls, and a closing surface at the nozzle entrance. The computation is conventionally made using the hypotheses of rigid walls, uniform speed of sound, and propagation through a medium at rest. Then the acoustic problem is reduced to the Helmholtz equation:

$$\begin{aligned} \Delta\bar{p}_N + \frac{\omega_N^2}{a^2}\bar{p}_N &= 0 \quad \text{in the cavity} \\ \frac{\partial\bar{p}_N}{\partial n} &= 0 \quad \text{on the surface} \end{aligned} \tag{8}$$

where ω_N appears as an eigenvalue. The perturbations brought by the incompressible ($M \ll 1$) mean flow, burning surfaces, and the nozzle, modify the wave equation to (here, a one-phase flow is assumed for brevity):

$$\begin{aligned} \Delta\tilde{p} + \frac{\omega^2}{a^2}\tilde{p} &= \tilde{h} \quad \text{in the cavity} \\ \frac{\partial\tilde{p}}{\partial n} &= -\tilde{f} \quad \text{on the surface} \end{aligned} \tag{9}$$

with

$$\begin{aligned} \tilde{h} &= (i\omega/a^2)\bar{\boldsymbol{u}}\cdot\nabla\tilde{p} - \bar{\rho}\nabla\cdot(\bar{\boldsymbol{u}}\cdot\nabla\tilde{\boldsymbol{u}} + \tilde{\boldsymbol{u}}\cdot\nabla\bar{\boldsymbol{u}}) \\ \tilde{f} &= i\omega\bar{\rho}\boldsymbol{n}\cdot\tilde{\boldsymbol{u}} + \bar{\rho}\boldsymbol{n}\cdot(\bar{\boldsymbol{u}}\cdot\nabla\tilde{\boldsymbol{u}} + \tilde{\boldsymbol{u}}\cdot\nabla\bar{\boldsymbol{u}}) \end{aligned} \tag{10}$$

Two perturbation parameters are used in the linearization process: ε for the amplitude of the oscillations and $\bar{M}$ for the Mach number of the steady flow. ω is now a complex number, $\omega = 2\pi f + i\alpha$.

Combining Eqs. (8) and (9) and taking a volume average over the volume V of the cavity of surface S, after some algebra and the use of the divergence theorem, one obtains the direct expression of ω as

$$\frac{\omega^2 - \omega_N^2}{a^2}E_N^2 = -\frac{i\omega_N}{a}\int_S (A + \bar{M})\bar{p}_N^2\,\mathrm{d}s \tag{11}$$

where A is the surface admittance $\bar{\rho}a(\bar{\boldsymbol{u}}\cdot\boldsymbol{n}/\bar{p})$, and $\bar{M}$ is the surface injection Mach number. The separation of the real

and imaginary parts of Eq. (11) leads to the expression for the amplification α in additive form, provided that $|\alpha| \ll \omega$:

$$\alpha = \sum_i \alpha_i$$

The following important assumption, to arrive at Eq. (11), must be noted:

$$\tilde{\boldsymbol{u}} \simeq \tilde{\boldsymbol{u}}_N = (i/\bar{\rho}\omega_N)\nabla\tilde{p}_N \tag{12}$$

Indeed, this cancels the terms resulting from the expansion and linearization of the

$$\boldsymbol{u}\cdot\nabla\boldsymbol{u} \equiv \tfrac{1}{2}\nabla\boldsymbol{u}^2 + (\nabla \wedge \boldsymbol{u}) \wedge \boldsymbol{u} \tag{13}$$

term in Eq. (10), therefore canceling all trace of vorticity of the flows, which seems to be overstated. The effects of the steady-state vorticity are discussed in Ref. 36.

Assumption (12) was indeed a reasonable one at times of Refs. 38–41, but this is no longer the case, due to the recent advances in understanding the unsteady velocity field, which turns out to be highly rotational, even in the absence of shed vortices in the flow.[42,43] An attempt to consider term (13), i.e., vorticity, in the acoustic balance was first proposed in Ref. 42 [see Eq. (5) of this reference], but no developments were given. It is proposed here to revisit this problem. Assuming that the unsteady velocity field is formed of the acoustic motions, as expressed by Eq. (12), and the vortical fluctuations, will invalidate assumption (12). The additional terms in Eq. (11), take the following form:

$$\bar{\rho}\left\{\int_V k_N^2[\tilde{\boldsymbol{u}}\cdot(\tilde{\boldsymbol{u}} - \tilde{\boldsymbol{u}}_N)]\tilde{p}_N \, dV + \int_V (\tilde{\boldsymbol{\Omega}} \wedge \tilde{\boldsymbol{u}})\, \nabla\tilde{p}_N \, dV + \int_V (\tilde{\boldsymbol{\Omega}} \wedge \tilde{\boldsymbol{u}})\cdot\nabla\tilde{p}_N \, dV\right\}$$

Concentrating on the last integral, which is closely related to the subject of vortex shedding, through Ω, it can be shown that, in the case of a two-dimensional flow, its integrand reduces to

$$-\tilde{\Omega}\tilde{v}\frac{\partial\tilde{p}_N}{\partial x} \tag{14}$$

It can be argued that this integrand takes significant values at localized points in the flow, such as the impact surface where $\tilde{v}$ and Ω are large, thus providing a natural way to introduce the acoustic coupling in the acoustic balance. In Eq. (14), the phase relationship between the impacting vortex and the acoustic field is clearly apparent, and a criterion, similar to the one arrived at in Sec. IV, can be derived. On that subject, Ref. 14 uses a similar approach, although it is different from the acoustic balance, and could explain the appearance of acoustic coupling in certain Strouhal number ranges.

VI. How to Make a Whistling Motor?

From all that precedes, one should be able to devise a whistling motor, by properly using the vortex-shedding phenomenon. This section describes how to do so, on the basis of the simple test case of Sec. III. Such a motor would be very interesting for studying unsteady phenomena inside solid propellant motors, without the need of external forcing, which is limited to laboratory scale setups. Should it be stressed, it is much more difficult to devise a motor that would not whistle at all!

First, a shear layer is needed as the source of vortices. Let's assume that a grain geometry is available that will produce a hyperbolic-tangent-like velocity profile that will be taken as a generic nondimensional profile $u/\Delta U = f(y/\delta)$. On that matter, the grain geometry of Fig. 3 is a good candidate.

Second, the hydrodynamic stability analysis can be performed on that profile, with the tools mentioned in Sec. III, namely an Orr–Sommerfeld solver, for the spatial growth rate theory. This will provide quasiuniversal curves, giving the dimensionless complex wave number, $a^r + ia^i$, as a function of the dimensionless frequency c^r. Figure 5 displays these curves for the velocity profile of Fig. 4. At this point, δ and ΔU_e are considered as free parameters, that can be used to translate c^r into actual frequency. Important results from these curves are the 1) value of c^r for maximum amplification: $(c^r)_{m/a}$; 2) the critical value of c^r, above which the shear layer is stable: $(c^r)_{cr}$; and 3) the dimensionless vortex displacement velocity $U_v/\Delta U_e = c^r/a^r = K_V$.

Third, the chamber length can be adjusted, so that the frequency f_p of the pth longitudinal mode of interest lies in the shear layer unstable range $[0, f_{cr}[$, or, preferably, is set to $f_{m/a}$. To do that, it is useful to express δ as a function of the chamber diameter D: $\delta = K_D D$, and to take ΔU_e proportional to the plug flow velocity U (or Mach number M) at the shear layer origin: $\Delta U_e = K_U U = K_U(a_0 M)$.

Once the nozzle throat diameter is fixed, M is easily determined from the one-dimensional mass balance. For a given geometry, K_D and K_U can be assumed to remain constant. This assumption should be checked, depending on the actual motor geometry.

As already mentioned, a necessary condition for instability is

$$(c^r)_p = (2\pi f_p \delta/\Delta U_e) < (c^r)_{cr} \tag{15}$$

For an acoustically closed cavity, the pth mode frequency is $f_p = pa_0/(2L)$, where L is the chamber length. Then substituting expressions for δ, ΔU_e, and f_p in (15) yields, after some rearrangements:

$$\frac{M}{p} > \frac{\pi K_D}{K_U(c^r)_{cr}}\left(\frac{D}{L}\right) \tag{16}$$

At this point, it is interesting to note that (16) provides an explanation for why motors with large L/D are prone to vortex shedding on their first longitudinal modes (small p).

Fourth, the standoff distance ℓ from the vortex generation point to the impact surface (e.g., the nozzle wall) should contain at least one vortex of wave length $\lambda_v (\lambda_v < \ell)$, with

$$\lambda_v = 2\pi\delta/(a^r)_p = K_V[2\pi\delta/(c^r)_p]$$

This yields another necessary condition, which reads, after some rearrangements:

$$\frac{M}{p} < \frac{1}{2K_U K_V}\left(\frac{\ell}{L}\right) \tag{17}$$

Then Eqs. (16) and (17) give the necessary conditions for instability in terms of the plug flow Mach number, which is easily adjustable:

$$p\frac{\pi K_D}{K_U(c^r)_{cr}}\left(\frac{D}{L}\right) < M < \frac{p}{2K_U K_V}\left(\frac{\ell}{L}\right) \tag{18}$$

Equation (18) leads to an existence condition that reads

$$1 < \frac{(c^r)_{cr}}{2\pi K_D K_V}\left(\frac{\ell}{D}\right) \tag{19}$$

Fifth, it is now a simple matter to adjust 1) the throat diameter and the grain length to achieve the right Mach num-

ber level M, 2) the chamber L/D ratio, and 3) the standoff distance ℓ, to satisfy (18).

It must be noted that conditions (15) and (17) can be expressed in terms of Strouhal numbers:

$$St_1 = (fD/U) < (K_U/2\pi K_D)(c')_{cr} \tag{20}$$

$$St_4 = (f\ell/U) > K_U K_V \tag{21}$$

Finally, it should be noted that Eqs. (18) or (20) and (21) are only necessary conditions, which may not be sufficient conditions for the vortex-shedding phenomenon to appear. However, experience gained at ONERA indicates that the physical phenomena have the necessary capacity to slightly adjust in a way that positive coupling will occur. This is why the inverse problem (how to make a stable motor) is very difficult, once these necessary conditions are satisfied.

Some application examples will be given below, on the basis of the velocity profile of Fig. 4, corresponding to the test case presented in Sec. III and described in Ref. 35. Figure 5 gives $(c')_{m/a} = 0.30$, $(a')_{m/a} = 0.75$, $(c')_{cr} \approx 1.60$, $(a')_{cr} = 3.20$, $K_V \approx 0.5$. Other useful values are $K_D = 0.22$, $K_U = 1.5$. Then Eq. (18) leads to

$$0.29p(D/L) < M < 0.67p(\ell/L) \tag{22}$$

and Eqs. (20) and (21) to $St_1 < 1.7$ and $St_4 > 0.75$.

Assuming that the vortices would be generated at the grain RHS corner, where the plug flow Mach number is close to 0.15 (see Ref. 35) yields:

$$D/L < 0.52/p \quad \text{and} \quad \ell/L > 0.22/p \tag{23}$$

This can be easily satisfied, and a first feasibility numerical test case,[18] was designed with $L = 400$ mm, $D = 90$ mm, $\ell = L/2$ ($D/L = 0.22$, $\ell/L = 0.50$) with similar M level, and exhibited a marked vortex-shedding phenomenon on the second mode ($p = 2$), which is compatible with (22) or (23) (see Sec. VII). Reference 18 applied Flandro's method to this test case and predicted a vortex-shedding driving on mode $p = 1$. To validate these results, an experiment was designed and test fired at ONERA,[21] with a nonmetallized propellant. Chamber dimensions were $L = 600$ mm, $D = 85$ mm ($D/L = 0.14$), overall grain length was 300 mm, so that $\ell \approx 300$ mm ($\ell/L \approx 0.50$). Plug flow Mach number M varied from 0.24 to 0.07 during the firing. Geometry was chosen so that the shearing conditions, at 6.5 mm burned, were similar to the conditions of the numerical test case of Ref. 18. Figure 6 shows the motor geometry and two of the griddings used for the numerical computations, at ignition time and at 11.5 mm burned (propellant thickness was 19 mm). Equation (18), with the particular conditions of this setup, reads $0.04p < M < 0.34p$, indicating that mode $p = 1$ can be excited throughout the firing. Figure 7 displays head-end and aft-end pressure measurements, as well as corresponding psds. On that figure,

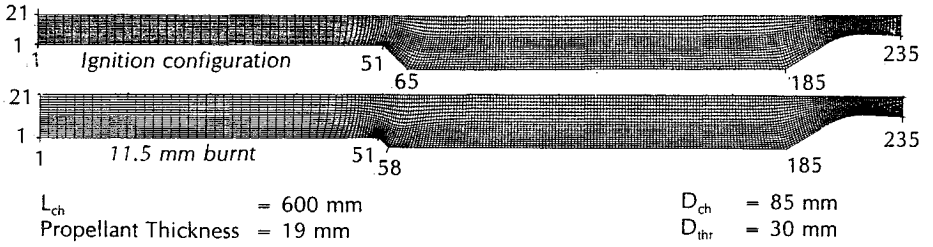

Fig. 6 Simple experimental whistling test motors from Ref. 21: geometry and grid at ignition and at 11.5 mm burned (propellant thickness 19 mm).

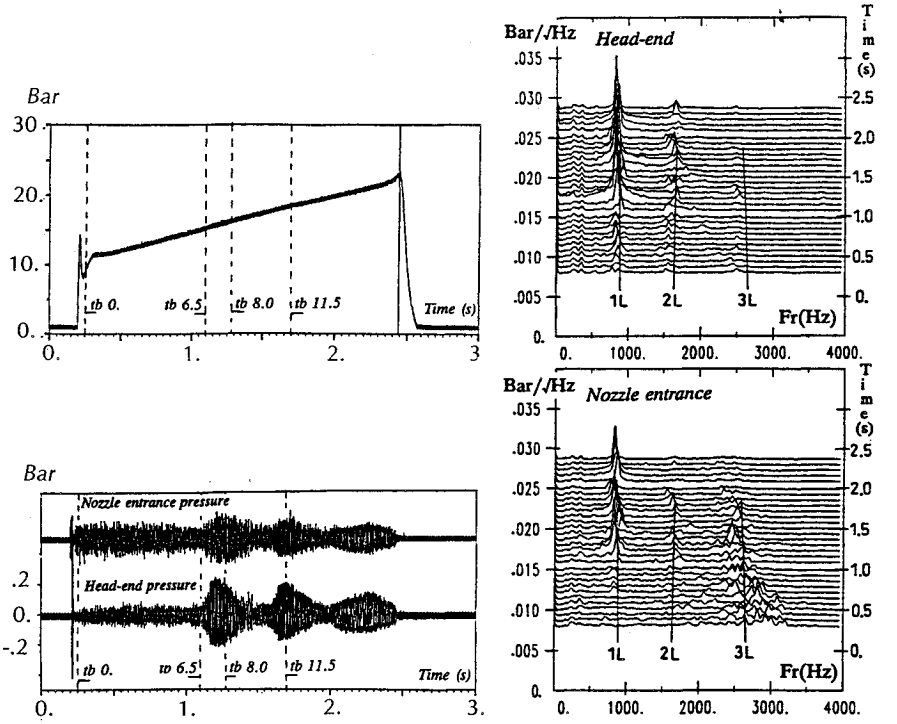

Fig. 7 Head-end and aft-end pressure measurements, waterfall plot of pressure psd. Experiment from Ref. 21.

the vortex shedding signature is clearly visible, mainly on mode $p = 1$, which is in good agreement with the simplified approach and Flandro's method. Comparisons with the full numerical approach will be discussed in Sec. VII. The appearance of mode 3 in the first part of the firing is less clear and it does not seem to properly couple (only visible at the aft end). This could be explained by the higher number of vortices being present (ℓ/λ_v of 4 is predicted) or by vortex destruction through turbulence, since high shear levels are achieved in the early part of the burn. However, this issue is still open to discussion.

In the second half of the firing, Fig. 7 displays the characteristic frequency cascade phenomenon, about the first mode frequency. This also can be explained with the simple arguments proposed previously. As the propellant burns, ℓ increases. To keep a given number of vortices present in the motor, their wavelength $\lambda_v = K_V[2\pi\delta/(c')_p]$ must grow, implying that $c'/\delta = 2\pi f/\Delta U_e$ should decrease. Since ΔU_e decreases with propellant regression, the frequency must also decrease. This happens until decoupling with the acoustics occurs. The number of vortices is then abruptly incremented of one unity, for identical ℓ, forcing a sharp reduction in λ_v, which, in turn, results in a sudden frequency increase. Then, the coupling can continue along another path, until further decoupling.

This section has shown that a rather satisfactory understanding of the physical mechanisms responsible for the vortex-shedding-driven oscillations can be obtained with limited tools in a simple situation. However, this is not sufficient, since in most cases these considerations are not taken into account during the motor design stages, and that oscillatory motors must be dealt with. In such conditions, prediction of unstable frequencies as well as oscillatory pressure and thrust levels, throughout the firing, is desirable, so that "best" or "better" conditions can be selected or proposed. In addition, it must be stressed that actual motor geometries are often complex and comprise multiple sources of shearing, and thus give rise to more complex phenomena. This motivates the efforts on full numerical approaches that will be described in the next section.

VII. Full Numerical Approaches

Although simplified approaches, such as those discussed in the preceding sections, are very useful in understanding the physical mechanisms responsible for vortex-shedding-driven oscillations in solid rocket motors, they fail to achieve reliable stability predictions in actual situations. Linearized methods can predict neither the precise actual frequency, nor the oscillatory levels, which are of primary importance for proper motor operation within given margins. Higher-order asymptotic expansions have been proposed in the literature, but they lead to complex developments and fix the choice of the relative orders of magnitude among various perturbation parameters. This introduces some degrees of arbitrariness. In that regard, full numerical solutions of the unsteady, compressible Navier–Stokes equations were proposed, as early as 1988, in the work packages relative to the Ariane 5 MPS P230 stability predictions. The arguments were that such methods would naturally include key mechanisms of vortex-shedding-driven oscillations, such as coupling of the acoustic field with shear layer instabilities, including nonlinear effects, and nozzle response to vortices. In that field, ONERA played a pioneering role in Europe that was rendered possible by the rapid development of computer codes and computer resources. In simple geometries, full unsteady computations of at least 10 oscillatory cycles, can be run in less than 10 min on a Cray Y-MP, which renders them quite affordable. At the time of this article, full unsteady computations are still limited to two-dimensional descriptions of the flow, due to heavy grid requirements and the long-time evolutions that are needed (at least 10 cycles) to describe the unsteady flow. However, three-dimensional computations are being considered in simple geometries and should become affordable in the near future. Assessing three-dimensional effects is really an important challenge. Indeed, when considering the spatial evolutions, from emission to impingement, of strong, primarily two-dimensional, vortices such as those computed in unstable motors (see below), the question of their stability should be addressed. The appearance of three-dimensional modes could modify the coupling mechanism.

To properly resolve important mechanisms such as shear layer instability and acoustic wave propagation, the requirements on the computer codes are severe. In this regard, it was decided in France, with the support of CNES, to start a workshop involving several national laboratories, with different codes, from CERFACS, CERMICS, ONERA/CERT/DERMES, SNPE, and ONERA. The workshop included three progressive numerical test cases, to validate the following points:

Test case no. 0: acoustic propagation, in a chamber with side injection, and development of the so-called acoustic boundary layers.[43] The grid was Cartesian with 5000 points.

Test case no. 1: vortex shedding in a chamber with a choked nozzle and side injection along two directions. The grid was curvilinear with 10,000 points.[18,19]

Test case no. 2: vortex shedding in an actual segmented 1/15-scale motor, with a submerged nozzle. The grid was a five-domains curvilinear grid, with up to 50,000 points.[20]

This workshop was very instructive and gave strong foundations for full numerical simulations of vortex shedding in solid rocket motors. Reference 44 gives an account of the lessons learned in the course of the workshop. These are summarized as follows:

1) Second-order-accurate, in time and space, schemes are necessary to properly capture the shear layers and acoustic motions.

2) Numerical dissipation and dispersion can influence the results and must be controlled. In particular, Van Leer's flux splitting turned out to be too dissipative to resolve the acoustic boundary layers, while Roe's flux splitting gave better results.

3) Implicit schemes were found to attenuate the acoustic waves, even at moderate time steps, so that only explicit schemes gave satisfactory results.

4) The correct behavior of the injecting boundary condition, in unsteady regimes, was found to be essential and had to be precisely checked.

5) On geometries with obstacles in the flow (such as inhibitor rings), where the sheared flow is produced by viscous boundary layers, cell Reynolds number limitations were encountered. This limited the actual scale of the computations on a given grid, or imposed grid refinements at a given scale.

6) Very good comparisons could be finally made between different family of codes (e.g., centered vs flux splitting schemes), once they were properly validated, on actual vortex shedding situations.

7) Differences could be observed among codes of the same family, depending on some particular numerical treatments. This point underlined the usefulness of the progressive test case approach, which provided a strong data base against which codes could be compared and evaluated.

Few examples will be given in the remainder of this section, to illustrate the potential of the numerical methods. These examples were computed with the ONERA SIERRA code, which uses the unsplit original Mc Cormack scheme to solve the two-dimensional Navier–Stokes equations in a finite volume, cell-centered, formulation.

The first example is the feasibility test case that was designed, with the simple tools of Sec. VI, to give rise to a vortex-shedding phenomenon. This test case is fully described in Ref. 18 for both the initial axisymmetric configuration and the latter two-dimensional planar configuration that was used

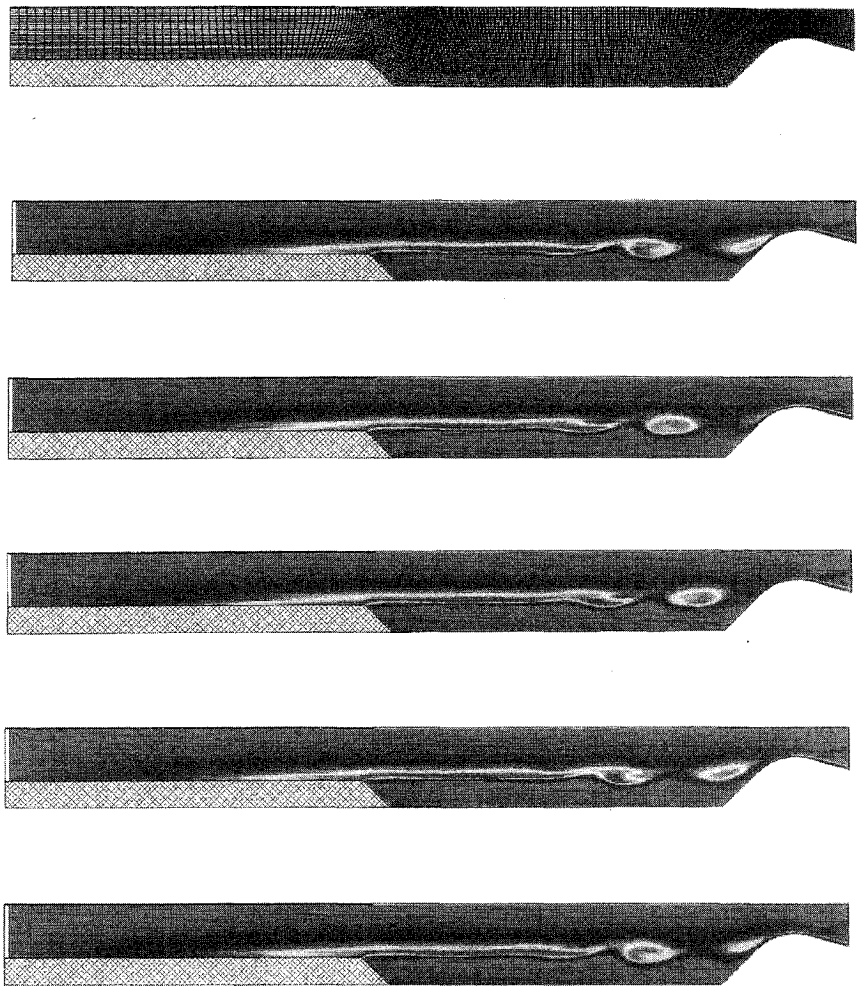

Fig. 8 First feasibility numerical test case and vorticity maps for the axisymmetric case. Computation from Ref. 18.

as test case no. 1 of the French numerical workshop. As mentioned in Sec. VI, this test case was based on the grain geometry displayed on Fig. 3, with an extended standoff distance, to lower the acoustic frequencies below the shear layer critical frequency (Fig. 5) and to provide sufficient space for the vortices to develop. From Sec. VI, the first two longitudinal acoustic modes have frequencies in the shear layer unstable range. All the numerical computations gave rise to a marked vortex-shedding phenomenon on the second acoustic mode at frequency of 2600 Hz, for both the axisymmetric and the two-dimensional planar cases. Figure 8 presents this test case and illustrates the vortex-shedding phenomenon. This test case was thoroughly studied at ONERA in the initial feasibility analysis. This work demonstrated that the full numerical approach was able to reproduce the frequency cascade phenomenon, as well as stabilization by decreasing the shear layer critical frequency below the first acoustic mode frequency.[27] Good agreement was also observed with the linear hydrodynamic stability analysis, in terms of vortical wavelength and vortex displacement velocity. These are important points that gave strong confidence in the full numerical approach, once properly mastered in terms of grid refinements and numerical diffusion errors. However, one point of dissatisfaction remained on why the second mode was excited, rather than the first one. As already mentioned in Sec. VI, Flandro's linearized approach predicted the first mode unstable and the second mode stable.[18] To clarify that matter, it was decided to conduct an experiment in an actual motor, as described in Sec. VI. This motor used the same generic grain geometry, adapted to existing hardware. Care was taken to ensure that shearing conditions, similar to the feasibility test case, were attained during the firing. This occurred at 6.5-mm propellant web thickness burned (total propellant thickness was 19 mm). This motor and the results from the firing are presented in Figs. 6 and 7. It is really amazing to note that the 6.5-mm-burned point corresponds to the appearance of a clear-cut case of vortex-shedding phenomenon about the first mode. Earlier into the firing, higher modes are present, from mode 2 to mode 3. Numerical computations were performed at four times into the firing (ignition, 6.5, 8, and 11.5 mm burned) and are presented in Ref. 21. These computations qualitatively recovered the experimental behavior. In particular, as initially anticipated, the 6.5-mm case computation was very similar to the feasibility test case one, with the second mode excited. Computations done at the two latter times correctly recovered the vortex-shedding phenomenon on the first mode, in good agreement with the experiment. Figure 9 illustrates this result for the 11.5-mm case. It is stressed in Ref. 21 that although satisfactory qualitative agreement was obtained between the computations and the experiment, the former failed to correctly predict the oscillatory levels. In particular, the ratio between the head-end and aft-end pressure levels was not correctly predicted. The previous two examples illustrate the rather good results obtained from basic internal aerodynamic codes, once properly validated, in simple configurations. In such geometries, the viscosity of the fluid plays a minor role, since the shear layers are produced inviscidly, from an injecting surface singular point (here, the RHS corner). Of course, the computer codes are presently lacking appropriate models for turbulence in unsteady regimes and for propellant response to oscillatory flows, so that quantitative predictions cannot be ensured at

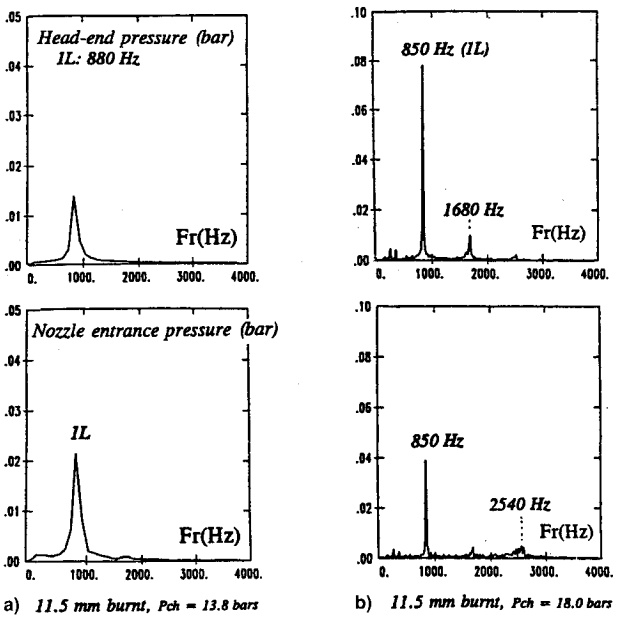

Fig. 9 Head-end and aft-end pressure spectra from a) computation and b) experiment, for the experimental motor of Fig. 6 at 11.5 mm burned, from Ref. 21.

the present time. This picture may not be so bright, when the shears layers are produced from obstacles in the flow, as it may be the case in actual segmented space boosters, where inhibitor rings are believed to protrude into the flow. Indeed, in such a case, the viscous boundary layers, developing along the obstacle walls, are the primary cause for sheared flow. This point was studied in test case no. 2 of the numerical workshop mentioned before. This test case was built from one of the parametric 1/15-scale segmented motors (LP3-A) that were fired at ONERA, which exhibited a marked vortex shedding phenomenon on mode 3, about the 20-mm-burned point.[20] In these motors, inhibitor rings were replaced by thick, thermally insulated, metallic diaphragms, so that their geometry could be known during all the firing. Figure 10 presents the particular geometry studied, together with the vortex shedding in the aft part of the motor, as illustrated from vorticity maps. In these computations, it is of primary importance to resolve the viscous boundary layer that develops on the diaphragm so that the computed velocity profile is physically meaningful. This constraint was translated in a cell Reynolds number limitation: $(Re)_{\text{cell}} = \rho|\Delta U_{\text{cell}}|\Delta_{\text{cell}}/\mu = \mathcal{O}(1)$, where ΔU_{cell} and Δ_{cell} are, respectively, representative of the velocity difference across the cell and of the cell size. For a given grid, this condition was forced by increasing the molecular viscosity μ by a constant factor K_μ. In the particular test case of Fig. 10, values of $K_\mu = 80$ were used for the fine

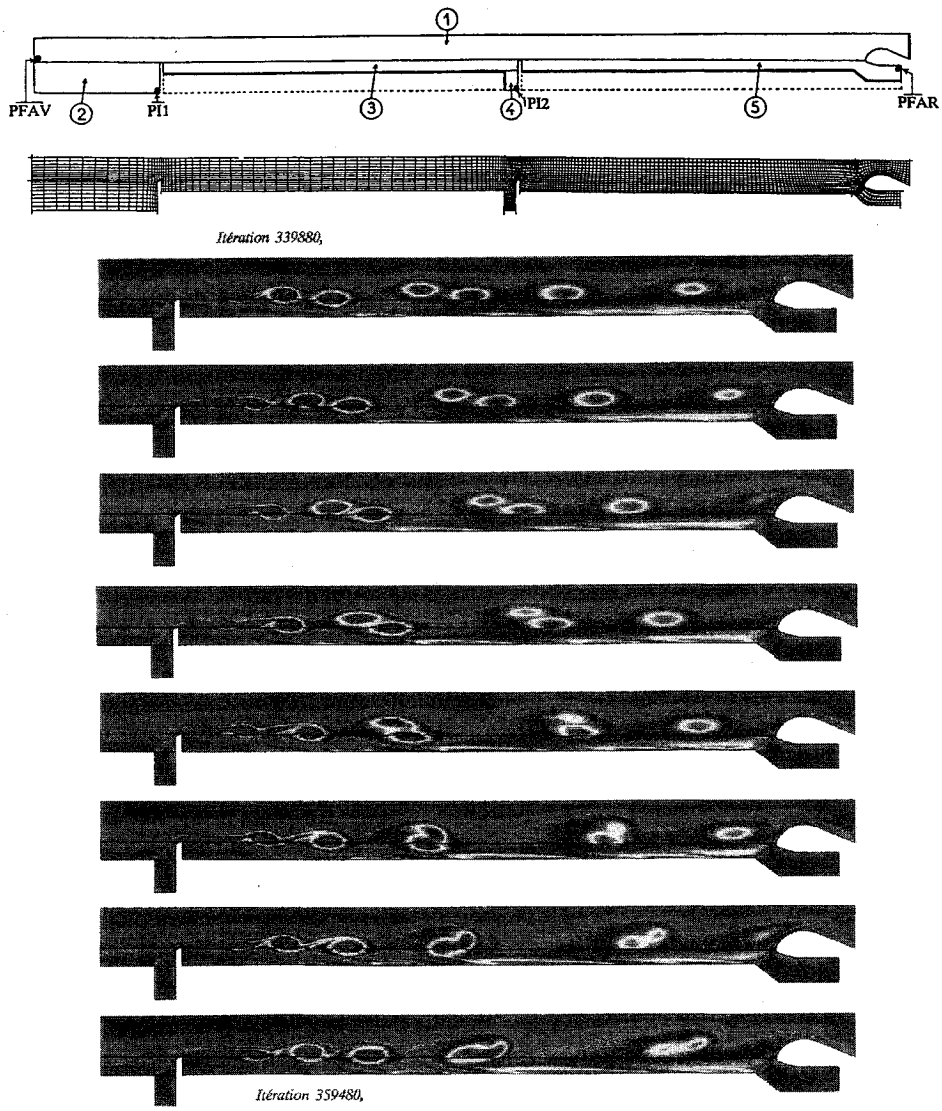

Fig. 10 Grid and domain arrangement for the LP3-A at 20 mm burned and example of self-excited unsteady solution, vorticity $\Delta T = 1/4(T_{3L}) = 0.278$ ms.

grid (50,000 points) and of $K_\mu = 400$ on the medium grid (12,500 points), for a motor length of the order of 1.5 m. This can be interpreted as a scale reduction by factor K_μ, or as an arbitrary way to introduce an extra diffusion that would result from turbulence in the flow. In any case, computations performed in the course of the workshop demonstrated that only when this condition was satisfied, good comparisons could be obtained between the different codes. Otherwise, the computed velocity profile was the result of numerical diffusion properties of each codes and the corresponding results did not compare well. This problem becomes of primary importance when full-scale computations are considered on "affordable" grids of less than 10^5 points, and when the protruding inhibitor rings are believed to be at the origin of the sheared flow. Despite these limitations, results from the full numerical computations, such as those of Fig. 10, are very valuable. As already mentioned, the vortex pairing, numerically observed in Fig. 10, was the key to explain the different frequencies experimentally observed at the motor aft end, which were puzzling, until the full computations became available. Here again, and despite the need to increase the molecular viscosity, the computational results were found to yield good qualitative comparisons with the experiment.[20]

The above examples show that the full numerical approach can give very valuable qualitative insights into unstable motor operation. Quantitative predictions of vortex-shedding-driven oscillations can now be foreseen, provided ad hoc models are used to include mechanisms that may affect the oscillatory levels or modify the conditions for vortex generation. Such mechanisms are two-phase flows, propellant combustion response to oscillatory conditions, turbulence, and in some conditions, the deformation of the inhibitor rings, under aerodynamic loads. The last two points appear to be the most challenging, since they are relatively new to the field of solid rocket motor stability analysis and since they are relevant to full-scale computations on actual segmented motors.

From the last test case, it becomes apparent that the precise shape of the obstacle is of primary importance on the shearing levels and vortex initial conditions. In an actual motor, on the contrary to the LP3-A 1/15 scale motor, the obstacles are made of thermal insulation materials that continuously ablate during the firing, raising the question of what diaphragm geometry should be used in the numerical computations. Moreover, the thermal insulation materials are usually soft materials whose moduli are relatively low and found to vary greatly with temperature. This makes the previous question even more difficult to answer, since the diaphragms are now susceptible to deform under the aerodynamic loads. The question of oscillatory motions of the diaphragms should also be raised. These problems have been known for several years,[2] but were not considered as relevant until recently. Indeed, Ref. 15 showed that similar vortex-shedding phenomena were observed for different diaphragm materials, including thermal insulation-like materials. More recently, the problem of fluid-structure interaction of solid rocket motor inhibitors was discussed in Ref. 45. Noticeable deformations were predicted, although the coupled computations were not carried out until convergence. Recent works at ONERA, carried out by P. Hervat, demonstrated the reality of large thermal insulation deflection, from a cold-flow experiment. This experiment reproduced a 1/15-scale condition with an actual thermal protection ring of thickness 4 mm. Figure 11 displays the main result of this experiment as inhibitor deflection vs pressure difference through it. At the same time, works performed by P. Y. Tissier and co-workers at SNPE demonstrated the feasibility to carry out the fluid-structure coupling until convergence and showed reasonable agreements with Hervat's experiment. As it now appears, the main difficulty in predicting the inhibitor ring shape and position is to precisely know its instantaneous geometry and thermal conditions. The possible response of the inhibitor ring to oscillatory flow conditions

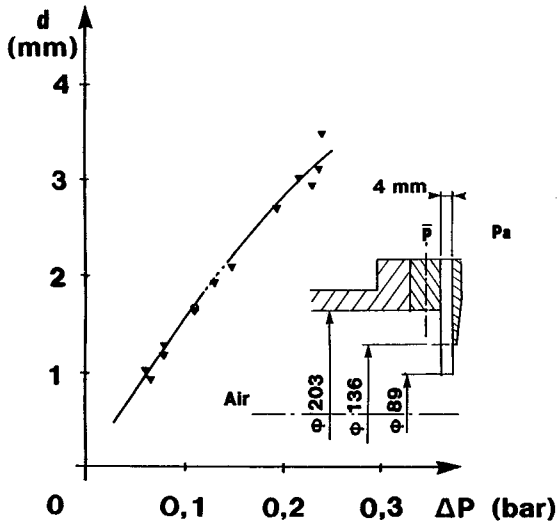

Fig. 11 Results from cold flow experiment on thermal insulation ring deflection under aerodynamic load, from P. Hervat (ONERA).

should be mentioned (or maybe the reverse should be considered: vortex-shedding driven by inhibitor ring oscillations?). Much work is needed before this problem can be satisfactorily addressed. However, the relevance of this problem is not yet quite clear. Indeed, it may turn out that, due to low modulus, high temperature, thermal degradation and ablation combined with high aerodynamic loads, the protrusion of inhibitor rings may be very marginal compared to other sources of shearing, such as port area discontinuities. This can be illustrated by Fig. 1 which corresponds to a 1/15-scale parametric motor (LP3-E) where the metallic diaphragm at the second intersegment (the one shown in Fig. 10) was removed. The observed vortex-shedding phenomenon closely resembles the behavior observed at the full scale.

The other point of turbulence modeling, in unsteady or oscillatory regimes, is also relevant to full-scale applications, where the Reynolds numbers are very large. In such conditions direct simulations could exceed, in grid and CPU time requirements, the available computer resources. Turbulence modeling in unsteady or oscillatory regimes requires some form of flow splitting, to separate the resolved part from the one that needs modeling. Two approaches are presently considered in France under support from CNES. The semideterminist approach[46] splits the flow in a coherent-resolved part and in an incoherent-modeled part. The modelization makes use of available two-equation turbulence models, such as the (k, ε) models, which are correspondingly modified. The large-eddy simulations[47,48] filters the flow in a low-frequency resolved part [noted hereafter $(\bar{\ })$], and provides a model for the high-frequency part. In most cases, the grid provides the so-called "natural filter," so that some form of grid control must be considered. Applications of such a model to two-dimensional cases, raise some conceptual problems, that must be mentioned and worked on.[49] However, the large eddy simulation technique seems to have many advantages for the considered applications. First, it preserves the distinctive unsteady nature of the computed flowfields. Second, the considered grids are already fine enough to capture all of the large-scale structures, so that grid refinements needed for LES may be limited. Finally, it can have some simpler forms that are readily applicable to existing laminar computer codes, so that their assessment can be done at a reduced cost. Two existing models, providing simple algebraic formula for the subgrid viscosity, are worth being briefly recalled as follows:

The most known Smagorinsky's model gives

$$\mu_{sg} = \rho(C_s\Delta_{\text{cell}})^2\sqrt{2\bar{s}_{ij}\bar{s}_{ij}}$$

where

$$\bar{s}_{ij} = \frac{1}{2}\left(\frac{\partial \bar{u}_i}{\partial x_j} + \frac{\partial \bar{u}_j}{\partial x_i}\right)$$

Lesieur's structure function model gives

$$\mu_{sg} = \rho(C\Delta)\sqrt{\langle \bar{F}_{2\Delta} \rangle}$$

where $\langle F_{2\Delta} \rangle$ is the average of the second-order-velocity structure function taken on surrounding cells and Δ is the average distance between surrounding cells:

$$\langle F_{2\Delta} \rangle = \frac{1}{4}\sum_{k=1}^{4} (\Delta U_k)^2 \quad \text{and} \quad \Delta = \frac{1}{4}\sum_{k=1}^{4} |\Delta r_k|$$

The constants C_s and C appearing in these models can be obtained from theoretical developments, which are valid for a three-dimensional homogeneous and isotropic turbulence in the Kolmogorov range. Usual values are $C_s = 0.18$, and $C = 0.063$. In two-dimensional configurations, these constants have no theoretical values, and should be estimated.[49] Here again, much work is still needed before this problem can be addressed satisfactorily in actual solid rocket motors. Precise cold-flow experiments seem the only way to validate the models, until velocity measurements can be performed in actual motors.

The other points of two-phase flow and propellant combustion response should pose less problems, since most of the background work is already available, and should become operational in the computer codes in the near future. Reference 50 demonstrated the feasibility to incorporate such phenomena in a one-dimensional numerical approach. For the two-phase flow issue, an Eulerian (two-fluid) approach seems to be the best suited to evaluate the influence of the most active particle-size class on the oscillatory levels. For the combustion response issue, some form of combustion modeling should be easily introduced in the boundary conditions on the propellant surface. On these subjects, the ultimate issue seems to be the distributed combustion (of the particular phase, e.g., aluminum) issue, which should be addressed once the previously mentioned two points are satisfactorily introduced into the codes.

VIII. Conclusions

The phenomena behind vortex-shedding-driven oscillations have been presented. It appears that simple tools are available that give the researcher or the design engineer valuable information on the mechanisms that control the appearance of oscillations. These tools, although limited, are essential to understand the mechanisms of vortex shedding and acoustic coupling.

Full numerical approaches have been shown to be very useful in providing unprecedented insight into oscillatory flowfields, and should become irreplaceable tools to predict motor stability, especially in geometrically complex situations. However, it has been shown that these methods should be first thoroughly evaluated and validated, in terms of unsteady behavior (boundary conditions, numerical diffusion errors) and grid requirements. Quantitative predictions of unstable frequencies and of pressure and thrust oscillatory levels, up to full-scale motors, can be envisioned in the near future. It must be stressed that full numerical approaches would only give global results, and thus, still need the physical understanding brought by simplified approaches.

In the past 20 years valuable progresses have been made in our understanding of vortex-shedding-driven oscillatory regimes. Several fields remain to be worked out, such as burning propellant response to oscillatory conditions, two-phase flow, turbulence modeling (which is essential to full-scale prediction), and the structural response of inhibitor rings, propellant grain or motor casing, to aerodynamic loads. These works will condition reliable quantitative predictions.

Acknowledgments

Most of the presented works have been made possible by support from BPD Contract 150085/LS, by delegation of ESA and under the supervision of CNES, and from CNES, R&T convention 89/3640 and Contract 93/7703. The whistling motor experiment was supported by ONERA. The continuous encouragement, help, and support of E. Robert from CNES and P. Kuentzmann from ONERA were very instrumental in this work and are kindly acknowledged. The author wants to acknowledge several years of work in common and many fruitful discussions with N. Lupoglazoff from ONERA, who also carried out all the numerical computations presented herein.

References

[1]Flandro, G. A., and Jacobs, H. R., "Vortex Generated Sound in Cavities," AIAA Paper 73-1014, Oct. 1973.

[2]Flandro, G. A., AGARD Consulting Mission to ONERA, Sept. 16–19, 1986.

[3]Kuentzmann, P., "Etudes Récentes à l'ONERA sur les Instabilités de Combustion dans les Moteurs-Fusées à Propergol Solide," *Solid Rocket Motor Technology*, AGARD CP-259, July 1979 (Paper 22).

[4]Kuentzmann, P., "Combustion Instabilities," AGARD LS 180, Sept. 1991.

[5]Mason, D. R., Folkman, S. L., and Behring, M. A., "Thrust Oscillations of the Space Shuttle Solid Rocket Booster Motor During Static Tests," AIAA Paper 79-1138, June 1979.

[6]Mathes, H. B., "Assessment of Chamber Pressure Oscillations in the Shuttle Solid Rocket Booster Motors," AIAA Paper 80-1091, June 1980.

[7]Dunlap, R., and Brown, R. S., "Exploratory Experiments on Acoustic Oscillations Driven by Periodic Vortex Shedding," *AIAA Journal*, Vol. 19, No. 3, 1981, pp. 408, 409.

[8]Brown, R. S., Dunlap, R., Young, S. W., and Waugh, R. C., "Vortex Shedding as a Source of Acoustic Energy in Segmented Solid Rockets," *Journal of Spacecraft and Rockets*, Vol. 18, No. 4, 1981, pp. 312–319.

[9]Alden, R. J., "Improved Performance 3.05 m (120 in.) Boosters for the Air Force Titan 34D Space Launch Vehicle," JANNAF Propulsion Meeting, 83N-35012, Vol. 1, 1983, pp. 15–27.

[10]Blomshield, F., and Mathes, H. B., "Pressure Oscillations in Post-Challenger Space Shuttle Redesigned Solid Rocket Motors," *Journal of Propulsion and Power*, Vol. 9, No. 2, 1993, pp. 217–221.

[11]Culick, F. E. C., and Magiawala, K., "Excitation of Acoustic Modes in a Chamber by Vortex Shedding," *Journal of Sound and Vibration*, Vol. 64, No. 3, 1979, pp. 455–457.

[12]Nomoto, H., and Culick, F. E. C., "An Experimental Investigation of Pure Tone Generation by Vortex Shedding in a Duct," *Journal of Sound and Vibration*, Vol. 84, No. 2, 1982.

[13]Isaacson, L. K., and Marshall, A. G., "Acoustic Oscillations in Internal Cavity Flows: Nonlinear Resonant Interactions," *AIAA Journal*, Vol. 20, No. 1, 1982, pp. 152–154.

[14]Hourigan, K., Welsh, M. C., Thompson, M. C., and Stokes, A. N., "Aerodynamic Sources of Acoustic Resonance in a Duct with Baffles," *Journal of Fluids and Structures*, Vol. 4, 1990, pp. 345–370.

[15]Flatau, A., "Vortex Driven Sound in a Cylindrical Cavity," Ph.D. Dissertation, Univ. of Utah, Salt Lake City, UT, March 1990.

[16]Flatau, A., and Van Moorhem, W., "Prediction of Vortex Shedding Responses in Segmented Solid Rocket Motors," AIAA Paper 90-2073, July 1990.

[17]Flandro, G. A., "Vortex Driving Mechanism in Oscillatory Rocket Flows," *Journal of Propulsion and Power*, Vol. 2, No. 3, 1986, pp. 206–214.

[18]Lupoglazoff, N., and Vuillot, F., "Numerical Simulation of Vortex Shedding Phenomenon in 2D Test Case Solid Rocket Motors," AIAA Paper 92-0776, Jan. 1992.

[19]Tissier, P. Y., Godfroy, F., and Jacquemin, P., "Simulation of Three Dimensional Flows Inside Solid Propellant Rocket Motors Using a Second Order Finite Volume Method—Application to the Study of Unstable Phenomena," AIAA Paper 92-3275, July 1992.

[20]Vuillot, F., Traineau, J. C., Prevost, M., and Lupoglazoff, N.,

"Experimental Validation of Stability Assessment Methods for Segmented Solid Propellant Motors," AIAA Paper 93-1883, June 1993.

[21]Lupoglazoff, N., and Vuillot, F., "Comparison Between Firing Tests and Numerical Simulation of Vortex Shedding in a 2D Test Solid Motor," AIAA Paper 93-3066, July 1993.

[22]Menon, S., and Jou, W. H., "Numerical Simulations of Oscillatory Cold Flows in an Axisymmetric Ramjet Combustor," *Journal of Propulsion and Power*, Vol. 6, No. 5, 1990, pp. 525–534.

[23]Farr, R. A., Nesman, T. E., Burnette, D., and Chasman, D., "Time-Accurate Navier-Stokes Computations of Low Speed Flow over Cavities: No-Slip vs. Blowing Walls," *Proceedings of the 4th International Symposium on Computational Fluid Dynamics* (Davis, CA), 1991, pp. 317–322.

[24]Farr, R. A., Nesman, T. E., Chasman, D., and Burnette, D., "Time-Accurate Navier-Stokes Computations: Dynamics of Pressure Oscillation in the RSRM 80 Seconds after Ignition," *Proceedings of the 4th International Symposium on Computational Fluid Dynamics* (Davis, CA), 1991, pp. 312–316.

[25]Zdravkovich, M. M., "Complementary Comment on "Review of Sound Induced by Vortex Shedding," *Journal of Sound and Vibration*, Vol. 99, No. 2, 1985, pp. 295–297.

[26]Blevins, R. D., "The Effect of Sound on Vortex Shedding from Cylinders," *Journal of Fluid Mechanics*,Vol. 161, 1985, pp. 217–237.

[27]Lupoglazoff, N., and Vuillot, F., "Analyse du vortex shedding par Simulation Numérique 2D dans un Propulseur à Propergol Solide et Calculs de Poussée Instationnaire," Colloque CNES-ONERA, Châtillon, France, Dec. 1992.

[28]Lin, C. C., *The Theory of Hydrodynamic Stability*, Cambridge Univ. Press, Cambridge, England, UK, 1955.

[29]Betchov, R., and Criminale, W. O., Jr., "Stability of Parallel Flows," Academic, New York, 1967.

[30]Varapaev, V. N., and Yagodkin, V. I., "Flow Stability in a Channel with Porous Walls," *Izvestiya Akademii Nauk SSSR, Mekhanika Zhidkosti i Gaza*, Vol. 4, No. 5, 1969, pp. 91–95.

[31]Michalke, A., "On the Inviscid Instability of the Hyperbolic-Tangent Velocity Profile," *Journal of Fluid Mechanics*, Vol. 19, 1964, pp. 543–556.

[32]Michalke, A., "On Spatially Growing Disturbances in an Inviscid Shear Llayer," *Journal of Fluid Mechanics*, Vol. 23, Pt. 3, 1965, pp. 521–544.

[33]Freymuth, P., "On Transition in a Separated Laminar Boundary Layer," *Journal of Fluid Mechanics*, Vol. 25, Pt. 4, 1966, pp. 683–704.

[34]Monkewitz, P. A., and Huerre, P., "Influence of the Velocity Ratio on the Spatial Instability of Mixing Layers," *Physics of Fluids*, Vol. 25, No. 7, 1982, pp. 1137–1143.

[35]Lupoglazoff, N., and Vuillot, F., "Simulation Numérique Bidimensionnelle des Écoulements Instationnaires dans les Propulseurs à Propergol Solide," La Recherche Aérospatiale, No. 1992-2, pp. 21–41.

[36]Culick, F. E. C., "Rotational Axisymmetric Mean Flow and Damping of Acoustic Waves in a Solid Propellant Rocket," *AIAA Journal*, Vol. 4, No. 8, 1966, pp. 1462–1464.

[37]Arnal, D., Habiballah, M., and Coustols, E., "Théorie de l'Instabilité Laminaire et Critères de Transition en Écoulement Bi et Tri Dimensionnel," La Recherche Aérospatiale, No. 1984-2, pp. 125–143.

[38]Hart, R. W., and McClure, F. T., "Theory of Acoustic Instability in Solid Propellant Rocket Combustion," 10th International Symposium on Combustion, The Combustion Inst., Pittsburgh, PA, 1965, pp. 1047–1065.

[39]Culick, F. E. C., "Acoustic Oscillations in Solid Propellant Rocket Chambers," *Astronautica Acta*, Vol. 12, No. 2, 1966, pp. 113–125.

[40]Culick, F. E. C., "The Stability of One-Dimensional Motions in a Rocket Motor," *Combustion Science and Technology*, Vol. 7, 1973, pp. 165–175.

[41]Culick, F. E. C., "The Stability of Three-Dimensional Motions in a Combustion Chamber," *Combustion Science and Technology*, Vol. 10, 1975, pp. 109–124.

[42]Brown, R. S., Blackner, A. M., Willoughby, P., and Dunlap, R., "Coupling Between Velocity Oscillations and Solid Propellant Combustion," AIAA Paper 86-0531, Jan. 1986.

[43]Vuillot, F., and Avalon, G., "Acoustic Boundary Layers in Solid Propellant Rocket Motors Using Navier-Stokes Equations," *Journal of Propulsion and Power*, Vol. 7, No. 2, 1991, pp. 231–239.

[44]Kourta, A., Carpentier, R., Larrouturou, B., Estivalezes, J. L., Godfroy, F., Tissier, P. Y., Lupoglazoff, N., and Vuillot, F., "Programme ASSM - Axe Stabilité de Fonctionnement: Synthèse des Résultats Acquis au Cours des Deux Premières Années," Colloque CNES-ONERA, Châtillon, France, Dec. 1992.

[45]Roach, R. L., Gramoll, K., Weaver, M., and Flandro, G. A., "Fluid-Structure Interaction of Solid Rocket Motor Inhibitors," AIAA Paper 92-3677, July 1992.

[46]Ha Minh, H., and Kourta, A., "Semi-Determinist Turbulence Modelling for Flows Dominated by Strong Organized Structures," *Proceedings of 9th Turbulent Shear Flows*, edited by Durst, Launder, Casagi, and Whitelaw, Vol. 1, Paper 10.5, Kyoto, Japan, Aug. 1993.

[47]Lesieur, M., *Turbulence in Fluids*, 2nd ed., Kluwer Academic, Norwell, MA, 1990.

[48]Comte, P., Ducros, F., Silvestrini, J., David, E., Lamballais, E., and Lesieur, M., "Simulation des Grandes Échelles d'Écoulements Transitionnels," 74th AGARD FDP Meeting, Chania, Crete, Greece, April 1994.

[49]Comte, P., private communication, June 1994.

[50]Levine, J. N., and Baum, J. D., "Modeling of Non-Linear Combustion Instability in Solid Propellant Rocket Motors," *19th International Symposium on Combustion*, The Combustion Inst., Pittsburgh, PA, 1982, pp. 769–776.